Journal of Hazardous Materials 418 (2021) 126223

Contents lists available at ScienceDirect

Journal of Hazardous Materials

journal homepage: www.elsevier.com/locate/jhazmat

Research Paper

Integrating multiple hybridization chain reactions on gold nanoparticle and alkaline phosphatase-mediated *in situ* growth of gold nanobipyramids: An ultrasensitive and high color resolution colorimetric method to detect the *mecA* gene of *Staphylococcus aureus*

Jing Zhou [a,b,c], Ruijie Fu [a,b,c], Haoran Liu [a,b,c], Yanlin Liu [a,b,c], Yiwen Wang [a,b,c], Bining Jiao [a,b,c], Yue He [a,b,c,1,*], Hongwu Tang [d,2,**]

[a] Citrus Research Institute, Southwest University, Chongqing 400712, PR China
[b] Laboratory of Quality & Safety Risk Assessment for Citrus Products (Chongqing), Ministry of Agriculture, PR China
[c] National Citrus Engineering Research Center, Chongqing 400712, PR China
[d] College of Chemistry and Molecular Sciences, Wuhan University, Wuhan 430072, PR China

ARTICLE INFO

Editor: Dr. Danmeng Shuai

Keywords:
Hybridization chain reaction
Gold nanomaterials
High visible-color resolution
Staphylococcus aureus
Alkaline phosphatase

ABSTRACT

Colorimetry has been considered as a potential instrument-free platform for point-of-care genomic detection. However, it is limited by the poor sensitivity and low color resolution. Herein, we report a high-resolution colorimetric biosensor based on multiple hybridization chain reactions (HCRs) on gold nanoparticle (AuNP) and alkaline phosphatase (ALP)-mediated *in situ* growth of gold nanobipyramids (AuNBPs) for ultrasensitive detection of the *Staphylococcus aureus* (*S. aureus*) *mecA* gene. In our design, target DNA is hybridized with capture hairpin DNA on magnetic beads and then amplified by multiple HCRs on AuNP. Since biotin-labeled hairpin-structured nucleic acids are utilized to conduct HCRs, together with the large specific surface area of AuNP, the biotin- and streptavidin- based reaction results in a large amount of ALP on AuNP. With the aid of NADPH, ALP-mediated *in situ* growth of AuNBPs is observed, and a series of rainbow-like colors are associated with different target DNA concentrations. Through the multiple-amplification strategy produced by AuNP, HCRs, and enzymatic reactions, the target DNA as low as 2.71 pM can be detected with high specificity. Moreover, this method has been successfully applied to detect the *mecA* gene extracted from *S. aureus*. Therefore, the proposed method holds great potential in clinical diagnosis.

1. Introduction

The occurrence and prevalence of antibiotic resistance have severely threatened public health. Among them, methicillin-resistant *Staphylococcus aureus* (*S. aureus*) is resistant to not only methicillin but also all other antibiotics (Stefani et al., 2012; Bulut et al., 2020). Thus, it can cause severe bacterial infection and is responsible for hundreds of millions of hospitalizations and deaths in human across the world every year. Gittens-St Hilaire et al. (2020) The methicillin resistance can be attributed to the *mecA* gene of *S. aureus*, which is a highly conserved sequence situated in the staphylococcal cassette chromosome *mec*. Ito et al. (2003) Therefore, early diagnosis of the *mecA* gene is essential to prevent and treat critical methicillin-resistant *S. aureus* infections. Currently, various analysis strategies exist for *mecA* gene detection, such as polymerase chain reaction (PCR) (Saka and Terzi, 2018) electrochemical biosensors (Xu et al., 2018; Liu et al., 2014), fluorescence methods (Shi et al., 2015; Li et al., 2018), surface plasmon resonance imaging (Nawattanapaiboon et al., 2015), sensors based on surface acoustic waves (Ji et al., 2020), and surface-enhanced Raman spectroscopy (Potluri et al., 2020). However, these analysis methods have a number of limitations; *e.g.*, they require expensive precision instruments and specialized personnel training. Consequently, their widespread

* Corresponding author at: Citrus Research Institute, Southwest University, Chongqing 400712, PR China.
** Corresponding author.
E-mail addresses: yuehe@cric.cn (Y. He), hwtang@whu.edu.cn (H. Tang).
[1] ORCID: 0000-0002-5727-7356
[2] ORCID: 0000-0002-2258-6992

https://doi.org/10.1016/j.jhazmat.2021.126223
Received 4 March 2021; Received in revised form 21 May 2021; Accepted 22 May 2021
Available online 3 June 2021
0304-3894/© 2021 Elsevier B.V. All rights reserved.

application in point-of-care detection is limited.

Colorimetric biosensors are currently attracting increasing amounts of attention because of their simplicity, rapid sensing, inexpensiveness, and visual signal output, and, therefore, they have great application potential in instrument-free point-of-care detection (Wang et al., 2020; Lai et al., 2017, 2016; Gao et al., 2017). Traditional colorimetric biosensors often suffer several disadvantages, *e.g.*, relatively low sensitivity and a single color readout that changes from light to deep, which limits their application (Jung and Park 2015; Luo et al., 2014; Li et al., 2009). In clinical diagnosis, the concentrations of genomic DNA are minimal, making it difficult to obtain detection signals. To improve detection sensitivity, researchers have developed a series of signal amplification strategies: loop-mediated isothermal amplification (Liu et al., 2018; Bao et al., 2020), hybridization chain reaction (HCR) (Dirks and Pierce, 2004), nicking enzyme signal amplification (Xu et al., 2009), rolling circle amplification (Xing et al., 2013), exonuclease III-assisted signal amplification (Cui et al., 2011), and catalytic hairpin assembly signal amplification (Chen et al., 2016). The HCR method has been extensively utilized for DNA amplification because of its mild reaction conditions, convenient operation, and high amplification efficiency. Choi et al. (2014) In a typical HCR, an initiator strand triggers a cascade hybridization reaction in the presence of two hairpin-structured nucleic acids (Gao et al., 2017; Hou et al., 2015) More importantly, HCR can progress spontaneously in an enzyme-free environment at room temperature, yielding a relatively long double-stranded DNA (dsDNA) nanostructure to amplify the detection signal (Dirks and Pierce 2004; Choi et al., 2014).

Recently, gold nanoparticle (AuNP) has been considered as an excellent nanocarrier to load large amounts of enzymes (or other molecules) to achieve signal amplification because of their large specific surface area, excellent biocompatibility, high stability, and convenient preparation and modification (Gao et al., 2013, 2014; Wu et al., 2015; Liu et al., 2010). In view of the above, by anchoring the initiator strand on the surface of AuNP to integrate the signal amplification capabilities of AuNP and HCR, we predict that multiple hybridization chain reactions (HCRs) will be progressed on AuNP, which will significantly improve the detection sensitivity of traditional colorimetric biosensors.

As mentioned earlier, another challenge is that traditional colorimetric biosensors only have a single color output, which seriously limits their visual detection accuracy and sensitivity (Liu et al., 2010; Chen et al., 2008). To improve visual resolution, Kou et al. (2006) utilized a target-triggered AuNP aggregation strategy to achieve a two-color output. In addition, Gao et al. (2017) developed a target-induced HCR strategy to consume hairpin DNA to trigger AuNP aggregation, thereby achieving a two-color output. Although this method improved the accuracy of visual detection to a certain extent, further improvements are required. Therefore, it is essential to construct a multicolor colorimetric method with a high visual resolution to visually inspect genomic DNA with excellent accuracy and sensitivity, to realize early identification of methicillin-resistant *S. aureus* infections.

Recently, gold nanomaterials have been extensively exploited to construct multicolor colorimetric biosensors, *e.g.*, gold nanospheres, gold nanocubes, gold nanobranches, gold nanorods, and gold nanobipyramids (AuNBPs), for two reasons: they have various morphologies that are easily tunable, and the adjustable localized surface plasmon resonance (LSPR) peak exists in a wide range from the visible region to the near-infrared region (Chen et al., 2008). Compared with other gold nanomaterials, AuNBPs have acquired widespread interest due to their higher extinction cross section, narrower plasmon line width, lower energy wavelength, and higher sensitivity to the refractive index (Kou et al., 2006; Liu et al. 2009). Therefore, AuNBPs are an ideal chromogenic substrate to construct multicolor colorimetric biosensors to detect a variety of substances, including influenza (Xu et al., 2017), glucose (Xu et al., 2019), ochratoxins (Wei et al., 2019), ferrous ions (He et al., 2020), and cyanide ions (Sasikumar and Ilanchelian, 2020). Regrettably, current approaches for synthesizing and purifying AuNBPs are typically very complicated and take a long time (approximately 3–4 days) (Li et al., 2015; Zhu et al., 2016; Qi et al., 2016). Recent studies have found that the *in situ* growth strategy can yield highly uniform AuNBPs without any purification steps. (Wang et al., 2019, 2020). For example, Wang et al. developed an alkaline phosphatase (ALP)-mediated *in situ* growth of AuNBPs strategy (Wang et al., (2019). Obvious color changes have been observed under different ALP concentrations. This strategy not only greatly improves the accuracy and sensitivity of visual detection, but also significantly reduces the synthesis time (3 days *vs.* 15 min) and the number of operation steps, making it promising for application in multicolor colorimetric assays.

Inspired by above evidence, herein, we integrated multiple HCRs on AuNP with ALP-mediated *in situ* growth of AuNBPs to develop a new colorimetric DNA biosensor with significantly improved sensitivity and visual color resolution. The high sensitivity of the multicolor colorimetric DNA biosensor is attributed to the perfect combination of superior AuNBPs properties and the three-round signal amplification strategy, which includes the use of AuNP as an initiator carrier for signal amplification, HCR amplification, and enzymatic signal amplification. To the best of our knowledge, this is the first intension to develop a multiple-amplification colorimetric DNA biosensor by fully integrating the outstanding properties of AuNBPs as a novel chromogenic substrate. Importantly, the multicolor readout used to detect DNA has great potential for point-of-care determination.

2. Materials and methods

2.1. Preparation of capture probe

Fig. S1 illustrated the construction of the capture probe. Basically, the capture probe was prepared based on the streptavidin-biotin interaction between the streptavidin-modified magnetic beads (SA-MBs) and the biotin-labeled capture hairpin DNA (CH DNA). The specific experimental steps for the preparation of capture probe were described as follows. After washing with coupling buffer, 200 μL of magnetic beads (MBs) (4 g/L) were incubated with 6 μL of 100 μM CH DNA at 25 °C for 30 min. Magnetic scaffold was used to adsorb MBs and remove the redundant CH DNA. After washing with coupling buffer for three times, the obtained capture probe was suspended in 200 μL coupling buffer.

2.2. Preparation of signal probe

As shown in Fig. S2, DNA 1 and DNA 2 were immobilized on AuNP by freezing-based labeling strategy (Hu et al., 2020). Both DNA 1 and DNA 2 were designed to have a poly (A) tail at the 3′ end. In addition, biotin-tagged hairpin DNA1 (H1) and biotin-tagged hairpin DNA2 (H2) were separately suspended in phosphate buffered saline with Tween (PBST) and kept at 95 °C for a period of 5 min, then gradually annealed to 25 °C to form stable hairpin structures. The specific experimental steps for the preparation of signal probe are described as follows. 5 μL of DNA1 (100 μM) and 5 μL of DNA2 (100 μM) were simultaneously added into 200 μL of AuNP solutions and mixed well. Then, the mixture was frozen at −80 °C for an hour. After thawing, the resulting DNA-labeled AuNP solution was washed twice with 0.1% Tween solution by centrifugation at 12,000 rpm/min for 30 min at 4 °C. Then the obtained AuNP was resuspended in 200 μL of PBST. Subsequently, 50 μL of H1 (20 μM) and 50 μL of H2 (20 μM) were added and incubated at 25 °C with continuous shaking for 90 min to progress multiple HCRs on AuNP. The resulting AuNP solution was washed twice with 0.1% Tween solution to remove any unreacted H1 and H2, and resuspended in 200 μL coupling buffer. After that, 3 μL of streptavidin-modified alkaline phosphatase (SA-ALP) was added to the above AuNP solution, and incubated at 25 °C for 40 min. Finally, 4 μL of streptavidin (1 mg/mL) was added to block the unreacted biotin sites. Thereafter, the obtained signal probe was washed twice and dispersed in 200 μL of the coupling buffer.

2.3. ALP detection

First, 50 μL of reaction buffer, which contained 50 mM L-ascorbic acid 2-phosphotrisodium salt (AAP) and various concentrations of ALP, were added in 12 centrifuge tubes, respectively. After 30 min of incubation at 37 °C, AAP was completely hydrolyzed to L-ascorbic acid (AA). Subsequently, 10 μL of 1.0 M HCl was employed to terminate the enzyme reaction and tune the pH to acidic condition (pH = 2.0). Then, the above solutions with a volume of 30 μL were respectively taken and mixed with 100 μL of monovalent gold element solution containing 1.25 μL of AuNBPs seed solution (the preparation step of monovalent gold element solution and AuNBPs seed solution were presented in the Supporting Information), followed by incubating at 55 °C for 15 min on the metal incubator. Finally, the solution color was recorded by the camera on a smartphone. Meanwhile, the ultraviolet−visible (UV−vis) absorption spectra was recorded.

2.4. Ultrasensitive multicolor colorimetric determination of target DNA

Different concentrations of target DNA were reacted with 15 μL capture probe and 15 μL signal probe at 25 °C for 15 min with gentle shaking. After washing three times with reaction buffer, the obtained capture probe/target DNA/signal probe complex was dispersed in 50 μL of reaction buffer containing 50 mM AAP. After incubation for 30 min at 25 °C with gentle shaking, the supernatant was collected by the assistance of magnetic separation for 30 s. Subsequently, 10 μL of 1.0 M HCl was added into the supernatant to terminate enzyme reaction and tune the pH (pH = 2.0). After that, the above solution with a volume of 60 μL was taken and diluted 10-fold with 1:5 ratio of HCl (1.0 M) and reaction buffer (pH = 2.0). Then, above solution with a volume of 30 μL was taken and mixed with 100 μL of monovalent gold element solution containing AuNBPs seed (1.25 μL), followed by incubating at 55 °C for 15 min on the metal incubator. Finally, the solution color was recorded by the camera on a smartphone. Meanwhile, the UV−vis absorption spectra was recorded by microplate reader.

To explore the specificity, oligonucleotides with partial/complete base mismatches were used for comparison with target DNA. In addition, four different concentrations of target DNA were spiked into milk to investigate the applicability of the developed biosensor in the real samples with complex biological matrix.

2.5. Detection of mecA-specific single-stranded DNA (ssDNA) of S. aureus

The culture was centrifuged at 6000 rpm/min for a period of 3 min to obtain *S. aureus* cells. Subsequently, 3 iron beads with a diameter of 3 mm were added into the centrifuge tube containing *S. aureus* cells. Then, *S. aureus* cells were grinded by Scientz-48 High-throughput Tissue Grinder. According to the instruction manual, the genomic DNA was extracted within 1 h using the TIANamp Bacterial DNA Kit. The PCR amplification of genomic DNA was achieved in a professional thermocycler. Specifically, PCR centrifuge tubes containing 10 μL of dNTP buffer and 6.6 μL ddH_2O, 1 μL of genomic DNA (50 ng/μL), 1 μL of primer F (10 μM), 1 μL of primer R(10 μM), and 0.4 μL of DNA polymerase. The PCR was performed at 94 °C for 3 min, followed by 33 cycles of 94 °C for 1 min, 60 °C for 1 min, 72 °C for 1 min, and 3 min extension. PCR products were characterized by running the samples in 2% agarose gel containing 4S green at a voltage of 100 V. Prior to the detection procedure, the PCR product was boiled at 100 °C water for 5 min, and quickly cooling in liquid nitrogen for 2 min to produce *mecA*-specific ssDNA. Then, the resulting *mecA*-specific ssDNA (445 ng/uL) was mixed with capture probe and signal probe to go through the detection steps.

3. Results and discussion

3.1. Sensing mechanism

The strategy mechanism was displayed in Scheme 1. The assay process included two parts: the hybridization process and the signal-producing process. In the hybridization process, CH DNA-immobilized MBs were utilized as capture probes. Then, by means of a freezing-based labeling method (Hu et al., 2020). two kinds of ssDNA, DNA1 and DNA2, were immobilized on the AuNP surface. In particular, DNA1 was designed as a complementary strand to part of CH DNA, whereas DNA2 was utilized as the HCR initiator. In addition, biotin-labeled hairpin-structured nucleic acids, H1 and H2, were employed to conduct the HCR, by which large amounts of ALP were anchored on AuNP based on the reaction of biotin and streptavidin. The obtained ALP- and DNA-conjugated AuNP was served as a signal probe. The presence of target DNA hybridized with CH DNA on the capture probe, producing a sticky end, which then went to the hybridization reaction with DNA1 on the signal probe (Fig. S3). The quick reaction response between the capture probe, target DNA, and the signal probe paved a smooth way for rapid target DNA detection. Besides, by using MBs as the reaction carrier ensured the detection of target DNA from complex matrices directly without complicate pretreatment. Moreover, multiple HCRs on the AuNP surface resulted in plenty of anchoring sites for ALP, which greatly improve the detection sensitivity. After the hybridization process, the assay went to the signal-producing process. Different from the previously reported method (Wang et al., 2019). It was found that coenzyme II reduced tetrasodium salt (NADPH) exhibited a better assistance effect on the ALP-mediated *in situ* growth of AuNBPs than reduced nicotinamide adenine dinucleotide I (NADH). Moreover, by using CTAB as an indicator, it is confirmed that the chemical valence of gold species produced by reducing chloroauric acid by NADPH is monovalent (Fig. S4). Therefore, NADPH was used to reduce trivalent gold element of chloroauric acid to monovalent at the first place in our work. As the substrate of ALP, AAP was introduced and then enzymatically transformed to AA. The obtained AA reduced the previously generated monovalent gold elements to zerovalent ones. The specific chemical reaction formulae are as follows:

$$\text{Au (III)} + \text{NADPH} \rightarrow \text{Au(I)}$$

$$\text{AAP} + \text{ALP} \rightarrow \text{AA}$$

$$\text{Au (I)} + \text{AA} \rightarrow \text{Au (0)}$$

Subsequently, zerovalent gold grown on the gold seeds and produced AuNBPs, which, in turn, resulted in significant color variation. In accordance with different colors and LSPR band shifts produced by the formed AuNBPs, an ultrasensitive visualization analysis of target DNA could be easily realized.

3.2. In situ growth of AuNBPs assisted by NADPH

As reported by Wang et al. (2019) that the AuNBPs can be prepared through ALP-mediated growth of AuNBPs. This *in situ* growth strategy can produce highly uniform AuNBPs, saving synthesis time and reducing number of operation steps. As our sensing principle is based on ALP-catalyzed AAP enzymatically transforming to AA, AA then induces AuNBPs growth. Therefore, the more sensitive of the *in situ* AuNBPs growth strategy is to AA, the better the performance for target DNA detection. According to the work of Wang et al. (2019) the bright yellow color of chloroauric acid exhibited obvious blank interference. To solve this problem, they employed NADH to reduce the trivalent gold elements of chloroauric acid to monovalent elements. Then, the addition of AA resulted in the growth of AuNBPs. Through the assistance of NADH,

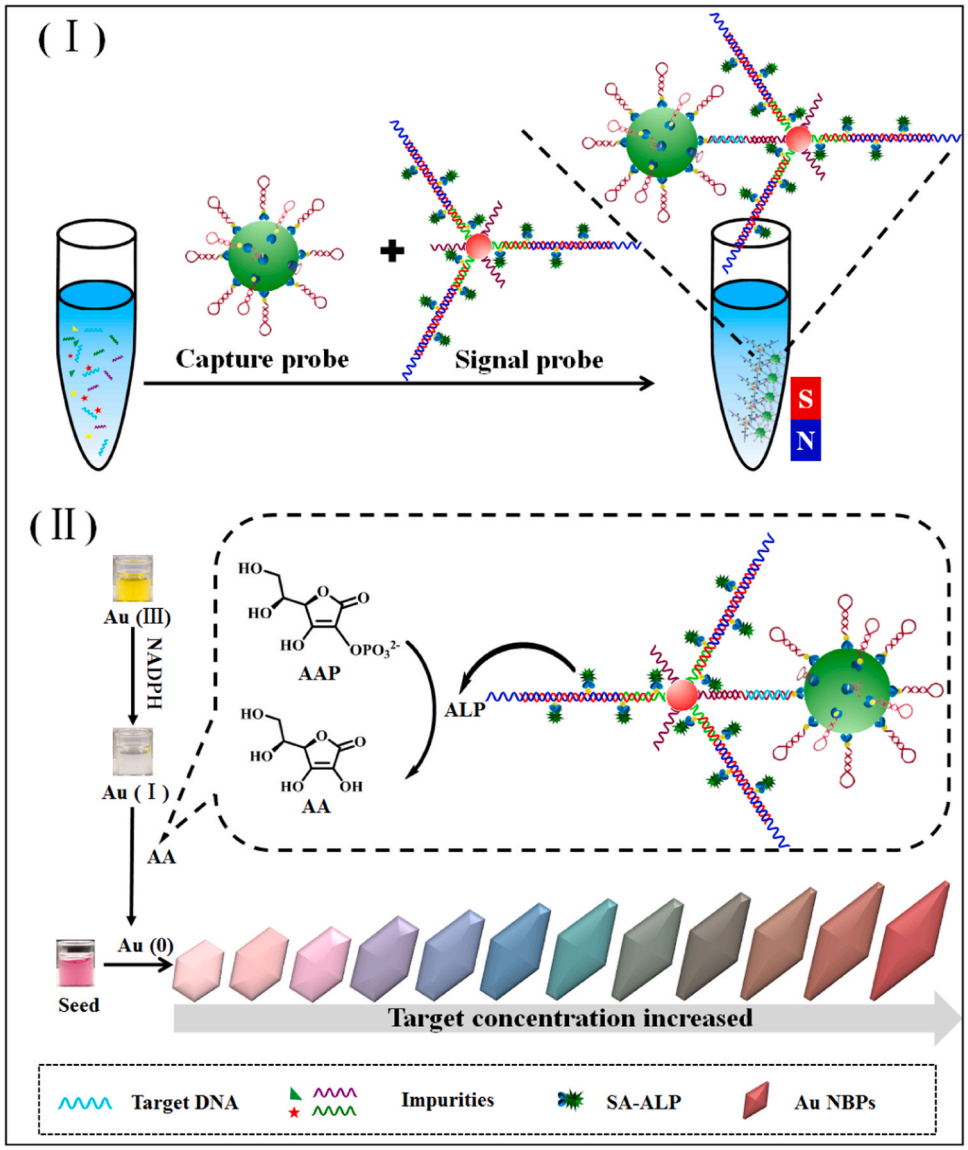

Scheme 1. Mechanism of the multicolor colorimetric DNA biosensor for visual determination of target DNA: (i) the hybridization process of capture probe, target DNA and signal probe; (ii) the signal producing process by using NADPH-assisted ALP-mediated *in situ* growth of AuNBPs.

the sensing solution with a colorless blank eliminated the blank interference. Consequently, a small amount of AA resulted in obvious color changes in the detection system, which shows high sensitivity toward AA. Inspired by the above work, NADPH, another reagent with a high reducing ability, was employed in our work to assist the AA-induced *in situ* growth of AuNBPs. The difference in assisting effects of NADH and NADPH was systematically investigated. As illustrated in Figs. S5A (a) and (b), with the aid of 2.0 mM NADH, as the concentration of AA increases, the AuNBPs solution has a distinct color change, in which the wavelength of longitudinal LSPR peak (λ_{max}) of AuNBPs changes from 540 to 770 nm. In this case, the original absorption wavelength of the gold seeds ($\lambda_0 = 530$ nm) was set as a reference (Fig. S6). As illustrated in Fig. S5A (c), the red-shift distance ($\Delta\lambda = \lambda_{max} - \lambda_0$) exhibits a good linear relationship when the concentration of AA increases from 20 to 300 μM; the corresponding calibration curve can be described by $y_1 = 0.818x + 1.487$, with an R^2 value of 0.992. Similarly, with the aid of 2.0 mM NADPH, the AuNBPs solution underwent obvious color changes when different concentrations of AA were added, as illustrated in Fig. S5B (a). The difference is that the same concentration of AA results in a larger shift of λ_{max}. Specifically, when the AA concentration increases from 20 to 300 μM, the longitudinal LSPR peak shifts from 540 to 950 nm, and the linear equation between Δλ and AA concentration can be described as $y_2 = 1.539x - 27.796$, with an R^2 value of 0.986, as illustrate in Figs. S5B (b) and S5B (c). The slope of y_2 is almost twice that of y_1. These results indicate that NADPH has a stronger assisting effect on the AA-induced *in situ* growth of AuNBPs than NADH. Therefore, NADPH was selected for further experiments in our work.

Under the assistance of NADPH, more detailed UV−vis absorption spectra and colors of AuNBPs solutions with AA concentration ranging from 19 to 308 μM were recorded. In particular, as illustrated in Fig. S7A, the AuNBPs solution displays 12 different colors, ranging from colorless to wine red with increasing concentration of AA. In addition, it was observed that the λ_{max} for AuNBPs increases significantly and finally reaches 950 nm (Fig. S7B). Moreover, a wide linear dynamic range was obtained (19–308 μM; Fig. S7C). These results indicate that the NADPH-assisted growth of AuNBPs is highly sensitive to AA.

Furthermore, transmission electron microscopy (TEM) images were employed to demonstrate the morphology of AuNBPs tuned by the concentration of AA with the assistance of NADPH. As displayed in Fig. 1A−E, as the concentration of AA increases, AuNBPs size also increases, albeit gradually; moreover, the AuNBPs morphology changes from irregular spheroid nanostructures to irregular hexahedron

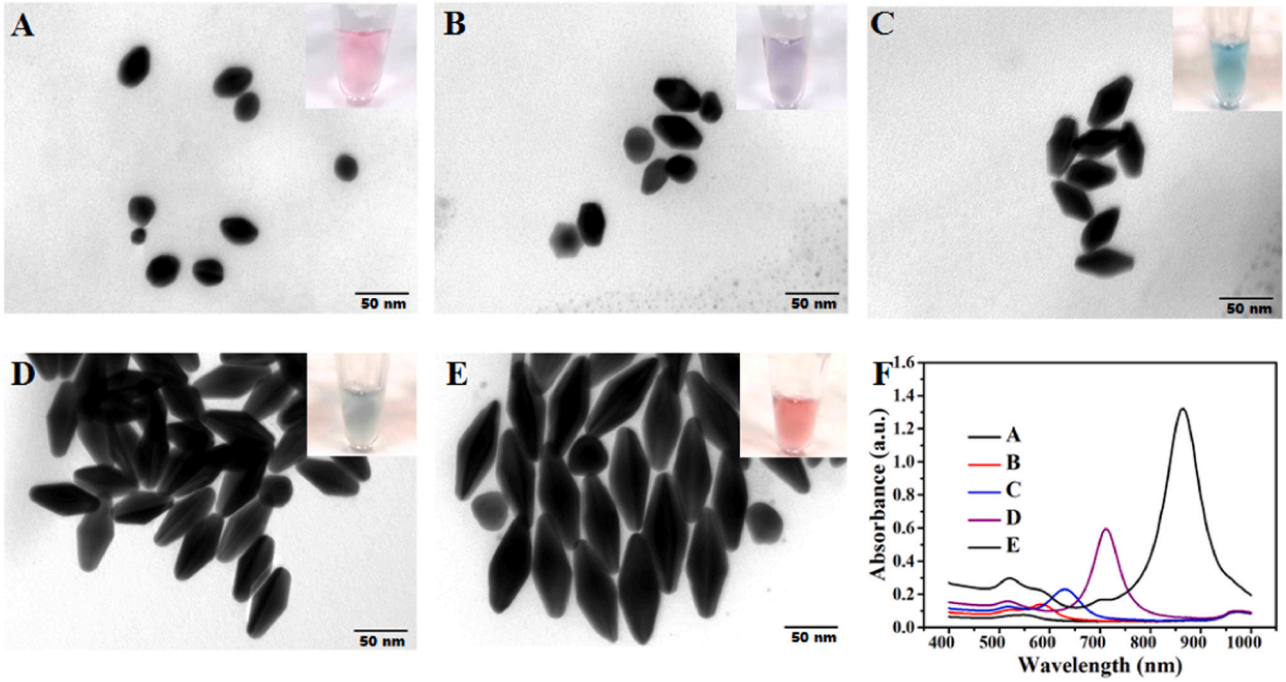

Fig. 1. (A–E) TEM images of the formed AuNBPs in the presence of different concentrations of AA with the help of NADPH (2.0 mM). Inset, the corresponding photographs. (F) their corresponding UV–vis absorption spectra. The AA concentrations from A to E were 38 μM, 69 μM, 96 μM, 115 μM, and 230 μM. (For interpretation of the references to colour in this figure, the reader is referred to the web version of this article.)

nanostructures, then to truncated bipyramid nanostructures, and finally to standard bipyramid nanostructures. Because of changes in AuNBPs morphology, the λ_{max} red shifts from 550 to 865 nm, which is accompanied by a color change from pink to bluish violet, to green, to grayish green, and then to wine red (Fig. 1F). It can be observed that the formed AuNBPs have high uniformity and a narrow plasmon line width, which results in bright colors in the detection solution that can be readily and accurately inspected with the bare eye.

3.3. Optimizing the preparation conditions for AuNBPs

To create superior AuNBPs, some experimental conditions were optimized. As we discussed earlier, NADPH was employed to reduce trivalent gold elements in chloroauric acid to monovalent elements and thus improve the sensitivity of *in situ* growth of AuNBPs to AA. Therefore, different concentrations of NADPH were investigated (0–4 mM), the results of which were illustrated in Figs. S8A and 8B. It is obvious that the λ_{max} increases with an increase in NADPH concentration. However, when the NADPH concentration is higher than 2 mM, the absorbance of the detection solution gradually decreases and is accompanied by a lighter color. Therefore, the optimal concentration of NADPH is 2 mM. Then, incubation temperature was altered to examine its influence on AuNBPs growth. As illustrated in Figs. S8C and 8D, the λ_{max} increases at first but then arrives at a maximum of 55 °C, after which the signal further decreases. Therefore, the optimal incubation temperature for AuNBPs growth is 55 °C. After that, the time for *in situ* growth of AuNBPs was optimized. As illustrated in Figs. S8E and F, the λ_{max} increases at first but then arrives at a maximum of 15 min, after which the signal gradually decreases. Therefore, the optimal time for *in situ* growth of AuNBPs is 15 min

AAP was introduced as the substrate of ALP and then enzymatically transformed to AA, which was used to induce AuNBPs growth by reducing the monovalent gold elements to zerovalent ones, which, in turn, resulted in significant color variation. By doing so, the AAP concentration was optimized. As illustrated in Figs. S8G and H, as the concentration of AAP increases from 0 to 50 mM, the λ_{max} increases, after which it decreases and essentially reaches equilibrium after 130 mM. In addition, the absorbance of the detection solution initially increases with an increase in AAP concentration and then gradually decreases after 50 mM. Hence, 50 mM is selected as the optimized concentration of AAP for further experiments. ALP has the best catalytic activity under alkaline conditions; however, a pH value that is too high will cause AA hydrolysis. Since AuNBPs growth is sensitive to pH (Qi et al., 2016), the HCl concentration was optimized to adjust the pH value of the reaction buffer after enzymatic reaction with ALP to further improve AuNBPs growth. To do this, HCl concentration was varied from 0 to 320 mM. As illustrated in Figs. S8I and J, the λ_{max} does not change much at first, but it gradually rises to a maximum of 240 mM, after which it gradually decreases. However, when the HCl concentration is 200 mM, the absorbance of the detection solution reaches a maximum and is accompanied by the brightest color output. Therefore, 200 mM HCl is chosen as the optimum concentration.

3.4. Assay of ALP activity

The relationship between the AuNBPs red-shift distance and ALP concentration under optimal conditions is illustrated in Fig. 2. As the ALP concentration increases from 0 to 15.4 U/L, the color of the AuNBPs solution changes significantly, and the longitudinal LSPR peak shifts from 530 to 800 nm (Fig. 2A and B). According to Fig. 2C, the red-shift distance of the longitudinal LSPR of AuNBPs possesses a good linear relationship with ALP concentration over the range of 0–15.4 U/L. The regression equation is $y = 17.535x + 9.365$ ($R^2 = 0.994$), with a limit of detection (LOD) of 0.17 U/L. The LOD of the proposed colorimetric DNA biosensor is calculated by 3S/slope, where S stands for the standard deviation of the blank group (n = 11). The color change of the detection solution can easily be observed with the naked eye when the ALP concentration is 0.8 U/L; this suggested that the visual detection limit is 0.8 U/L for ALP. The proposed multicolor colorimetric DNA biosensor not only exhibits many colors but also has a comparable (or even higher) sensitivity to those of other methods (Table S2). The high sensitivity of the proposed NADPH-assisted strategy of *in situ* growth of AuNBPs to

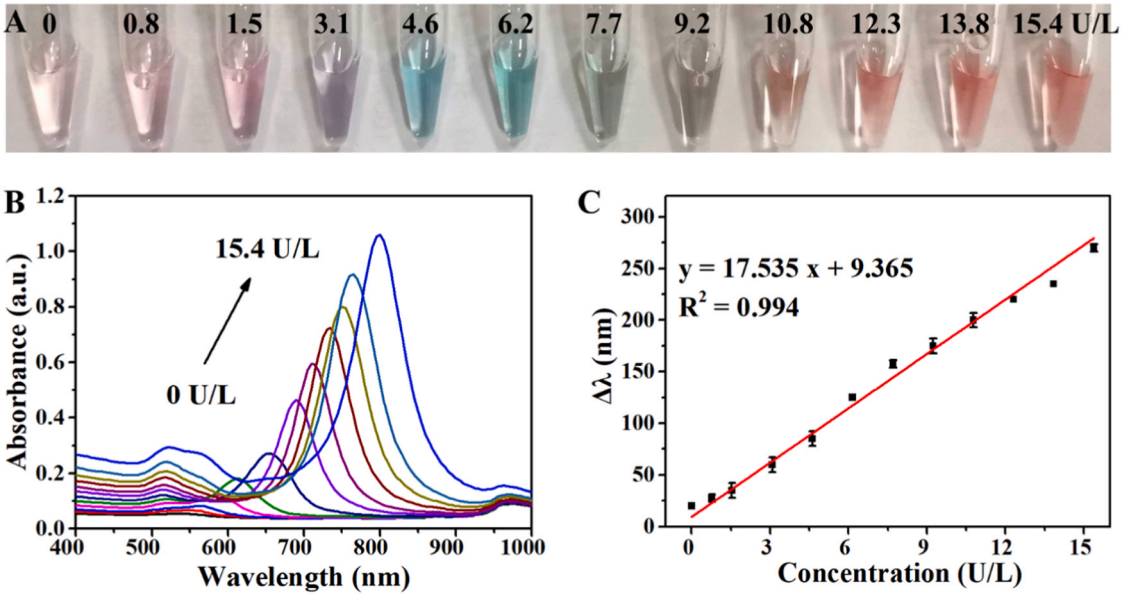

Fig. 2. (A) Pictures and (B) UV−vis absorption spectra of AuNBPs when different concentrations of ALP are introduced. (C) The linear curve between △λ and ALP concentration. (For interpretation of the references to colour in this figure, the reader is referred to the web version of this article.)

ALP is beneficial to the detection of target DNA.

3.5. Signal probe study

DNA1 and DNA2 were immobilized on the AuNP surface using a freezing-based labeling method (Hu et al., 2020). As displayed in Fig. S9, both the naked AuNP and DNA1/DNA2-labeled AuNP have good dispersibility in water (curves a and b and solutions a and b). As illustrated in Fig. S9 (curve c and solution c), the bare AuNP aggregated rapidly in the high-salt solution. Conversely, when the AuNP surface was labeled with DNA1 and DNA2, the obtained AuNP still had good dispersion (curve d and solution d). This result indicates that the surface of AuNP is modified with DNA1 and DNA2 successfully due to the highly stability of DNA1/DNA2 modified AuNP in high salt solution. In addition, from the dynamic light scattering results, larger hydrodynamic diameters and more negative zeta potential values can be observed after the AuNP was labeled with DNA1 and DNA2 (Table S3), further indicating that DNA1 and DNA2 were successfully labeled on the AuNP surface by the freezing-based labeling method.

Since DNA1 was designed as a complementary strand to part of CH DNA on MBs, DNA2 was utilized as the HCR initiator. Therefore, the DNA1−DNA2 concentration ratio is a key influencing factor of the detection performance of the proposed method. Accordingly, the capture probe, target DNA, and DNA1/DNA2-labeled AuNP were mixed to investigate the influence of the DNA1−DNA2 concentration ratio on the capture efficiency toward DNA1/DNA2-AuNP. After magnetic separation, the characteristic absorption peak value of AuNP at 520 nm in the supernatant decreases as the DNA1 concentration increases (Fig. S10A). This result indicates that the hybridization reaction between target DNA and capture probe opened CH DNA, and further hybridized with DNA1, causing the capture probe to pull down DNA1/DNA2-AuNP. Therefore, with an increase in DNA1 concentration, the number of captured AuNP increases. However, excessive DNA1 can reduce the amount of DNA2 immobilized on the AuNP, which, in turn, reduces the amount of HCR on the AuNP and ultimately affects the output signal. Therefore, the influence of the DNA1−DNA2 concentration ratio on the output signal required further investigation. Before the said investigation was conducted, gel electrophoresis was performed to prove that DNA2, H1, and H2 facilitated HCR successfully, and, in doing so, dsDNA with a high molecular weight was obtained in 0.1 M PBST (Fig. S11). As illustrated in Figs. S10B and C, regardless of whether the target DNA concentration is low or high, the AuNBPs mediated by the signal probe labeled with a DNA1–DNA2 concentration ratio of 1:1 have the largest absorbance intensities and wavelength of longitudinal LSPR peaks. Therefore, the optimal DNA1−DNA2 concentration ratio is 1:1.

3.6. Verification of signal amplification by AuNP and HCR

To verify signal amplification by AuNP, biotin-labeled DNA1 was introduced to hybridize with the target DNA and CH DNA on the capture probe. Then, SA-ALP was captured on the surface of MBs through the interaction between biotin and streptavidin (Fig. S12A). Thereafter, ALP mediated the *in situ* growth of AuNBPs. The obtained AuNBPs were characterized by UV−vis absorption spectra. Fig. S13A (curve a) displays that the characteristic absorption peak of AuNBPs cannot be observed, which indicates that the ALP concentration captured by MBs was too low to mediate AuNBPs growth. However, after fixing DNA1 and biotin-labeled DNA2 on the AuNP surface, it then interacted with SA-ALP (Fig. S12B). The obtained AuNP-ALP was used to detect target DNA. As illustrated in Fig. S13A (curve b), the λ_{max} is much higher than that of curve a, indicating that AuNP with a high specific surface area provides plenty of anchor points for ALP, which, in turn, significantly improve the detection sensitivity. Furthermore, to verify the signal amplification by HCR, DNA2 immobilized on the AuNP surface was designed as an initiator to trigger multiple HCRs. Since the two hairpin-structured DNAs, H1 and H2, were labeled with biotin, a huge number of anchor sites for SA-ALP were generated by multiple HCRs on the AuNP. As illustrated in Fig. S13A (curve c), the longitudinal LSPR peak further red-shifts compared with that illustrated by curve b. In addition, the λ_{max} produced by the aforementioned three groups were examined to calculate their p-values. In the histogram, p-values were marked with an asterisk (*, $0.01 < p < 0.05$; **, $p < 0.01$). As displayed in Fig. S13B, there is a significant difference between the group with signal amplification by AuNP and HCR and the other two groups. These results demonstrate that the detection signal was successfully amplified by the large specific surface area of the AuNP and by multiple HCRs.

3.7. Analysis of target DNA

Based on the exquisite combination of the superior properties of

AuNBPs and three-round of signal amplification strategy, the proposed method for the determination of target DNA was constructed. As displayed in Fig. 3A, as the target DNA concentration changes from 0 to 800 pM, the color of the solution varies: pink, blue, light green, olive, grayish green, yellow, and wine red. Importantly, the target DNA concentration can be easily distinguished between 0 and 10 pM by the naked eye. Therefore, the visual detection limit of target DNA is 10 pM. Moreover, the longitudinal LSPR peak red-shifts significantly from 570 to 870 nm (Fig. 3B). The relationship curves between the λ_{max} of AuNBPs and target DNA concentrations are presented in Fig. 3C, from which it is evident that when the concentration increases from 10 to 100 pM, the λ_{max} rapidly increases. When the target concentration increases to 100 pM, the increase in the λ_{max} is relatively slow relative to the increase rate of the target DNA concentration. By plotting the target DNA concentration *vs* the wavelength of the longitudinal LSPR peak of AuNBPs, two calibration curves were obtained. One of them is that when the concentration of target DNA increases from 10 to 100 pM, the corresponding calibration curve can be described by $y1 = 1.012x1 + 586.438$ with an R^2 value of 0.997. The other one is that when the concentration of target DNA increases from 100 to 600 pM, the corresponding calibration curve can be described by $y_2 = 0.318x_2 + 667.107$, with an R^2 value of 0.981. The LOD of the proposed method for target DNA is 2.71 pM. For each concentration of target DNA, we repeated the measurement at least 3 times independently. Table S4 shows the relative standard deviation (RSD) of the λ_{max} values of target DNA at different concentrations. The average RSD is 0.72%, which indicates excellent repeatability of this method for target DNA detection. Compared with other DNA detection methods, the developed multicolor colorimetric DNA biosensor not only has abundant color changes, but it is also at least an order of magnitude lower than other colorimetric methods (Table S5); moreover, it is even better than some electrochemical methods and fluorescence methods (Table S6). In addition, the cost of this colorimetric DNA biosensor for testing a single sample is only ~USD $1.43 (Tables S7 and S8). The above results illustrate that the proposed method is promising for the early monitoring of *S. aureus*.

Furthermore, the specificity of the proposed multicolor colorimetric DNA biosensor was appraised by investigating a series of solutions containing DNA with n base mismatch and the random DNA sequence (blank) under the same conditions (where n = 1, 2, 3, and 4, corresponding to M1, M2, M3, and M4, respectively). As depicted in Fig. 4A and B, the corresponding λ_{max} of the detection solution decreases significantly with an increase in the number of mismatches. The λ_{max} for detecting target DNA reaches 930 nm, whereas that of single-base mismatched DNA decreases to 697 nm. The corresponding longitudinal

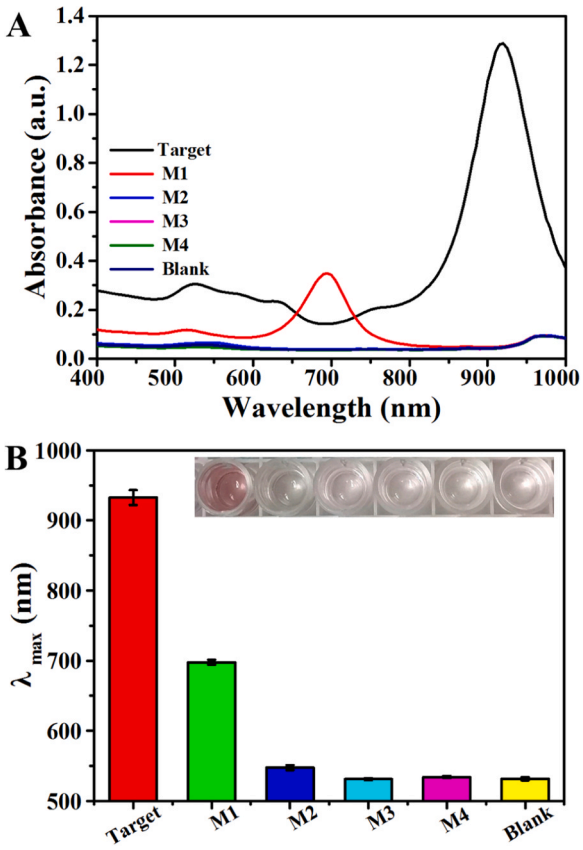

Fig. 4. (A) UV−vis absorption spectra and (B) histogram were obtained by detecting partially/completely noncomplementary DNA (M1: DNA with one-base mismatch, M2: DNA with two-base mismatch, M3: DNA with three-base mismatch, M4: DNA with four-base mismatch, blank: the random DNA sequence). The concentration of target DNA and all other partially/completely noncomplementary DNA were 100 nM.

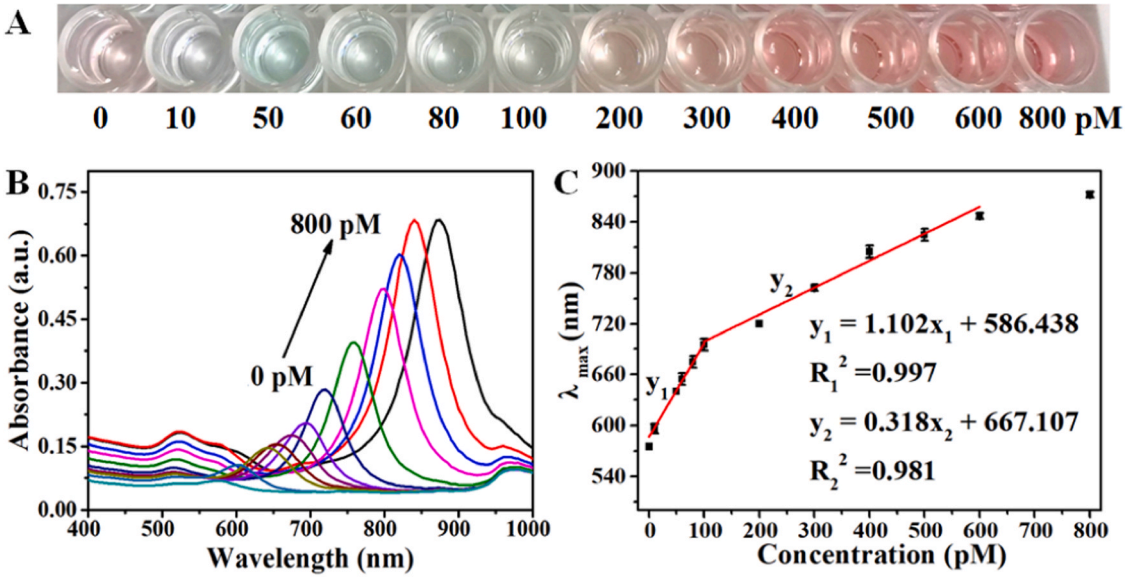

Fig. 3. (A) Pictures and (B) UV−vis absorption spectra of AuNBPs when different concentrations of target DNA are introduced. (C) The linear curve between λ_{max} and target DNA concentration. (For interpretation of the references to colour in this figure, the reader is referred to the web version of this article.)

Table 1
Recovery results of target DNA spiked in milk samples based on the proposed multicolor colorimetric DNA biosensor.

Samples	Added (pM)	Color	Measured (pM)	Recovery (%)	RSD (n=3,%)
Milk	500		489.58	98	6.63
	80		82.37	103	2.99
	30		32.54	108	1.50
	10		11.55	115	1.20

LSPR peak for AuNBPs containing M2, M3, and M4 is comparable to that of the random sequence group. Therefore, our proposed multicolor colorimetric DNA biosensor exhibit high specificity.

3.8. Analysis of target DNA in real samples

To investigate whether the developed multicolor colorimetric DNA biosensor was suitable for the determination of target DNA in real samples, different concentrations of target DNA (10, 30, 80, and 500 pM) were spiked in milk to perform recovery experiments. Prior to analysis, an un-spiked milk sample was investigated. As shown in Fig. S14, the milk sample exerts negligible influence. As illustrated in Table 1, the recovery rates for all spiked samples are between 98% and 115%, and the relative standard deviations are between 1.20% and 6.63%. It can be concluded that the possible interference of milk was eliminated by magnetic separation. This above data proved that taking MBs as reaction carrier ensured the direct detection of target DNA from complex matrixes directly without complicate pretreatment.

3.9. Analysis of mecA–specific ssDNA of S. aureus

To investigate the potential applicability of the developed multicolor colorimetric DNA biosensor, the PCR products of *S. aureus* genomic DNA were analyzed under the same conditions as those of the artificial target DNA detection. The agarose-gel electrophoresis image of PCR products at different concentrations is presented in Fig. S15A. As the loading concentration of PCR products increases, the corresponding characteristic bands become brighter. The performance of the proposed colorimetric DNA biosensor with respect to detecting *mecA*-specific ssDNA was also analyzed. As illustrated in Fig. S15B, as the clarity of the band in the agarose-gel electrophoresis image increases, the λ_{max} increases. In addition, the color of the solution changes with changes in the concentration of *mecA*-specific ssDNA (Fig. S15C). Therefore, the proposed multicolor colorimetric DNA biosensor was expected to be an effective strategy for determination of the said sequence.

4. Conclusion

In summary, a colorimetric DNA biosensor with a high color resolution and ultra-sensitivity was developed for the first time for *mecA* gene of *S. aureus* detection by combining multiple HCRs on AuNP with the NADPH-assisted ALP-mediated *in situ* growth of AuNBPs. By exploiting the amplification effects of the large specific surface area of AuNP, HCRs and enzymatic reactions, the artificial target DNA was identified at a low detection limit of 2.71 pM. In addition, the outstanding AuNBPs optical properties and fast response of the NADPH-assisted *in situ* growth strategy resulted in rich color changes for the detection system at different artificial target DNA concentrations for a total detection time of 1 h. Moreover, when the proposed biosensor was applied to the detection of artificial target DNA in milk, its excellent recovery rate and no need for complicated sample pre-processing and large instruments indicated that the proposed method holds a great potential in instrument-free point-of-care detection. Importantly, the proposed multicolor colorimetric DNA biosensor performed well in detecting the extracted *mecA*-specific ssDNA from methicillin-resistant *S. aureus*, suggesting that it holds promising application prospects for *S. aureus* detection in clinic diagnosis. With the merits of ultra-high sensitivity, rich color signal output, strong anti-interference ability, excellent applicability, the proposed multicolor colorimetric DNA biosensor can provide a simple and versatile pathway for early detection of nucleic acids.

CRediT authorship contribution statement

Jing Zhou: Conceptualization, Investigation, Data curation, Writing - original draft. **Ruijie Fu**: Software. **Haoran Liu**: Formal analysis. **Yanlin Liu**: Methodology. **Yiwen Wang**: Resources. **Bining Jiao**: Funding acquisition. **Yue He**: Conceptualization, Methodology, Supervision, Writing - review & editing. **Hongwu Tang**: writing - review & editing, Funding acquisition.

Declaration of Competing Interest

The authors declare that they have no known competing financial interests or personal relationships that could have appeared to influence the work reported in this paper.

Acknowledgment

This work was financially supported by the National Risk Assessment Program for Agricultural Products Quality and Safety, China (GJFP2019012), China Agriculture Research System, China (CARS-26) and the National Natural Science Foundation of China, China (81772256 and 21827808).

Appendix A. Supporting information

Supplementary data associated with this article can be found in the online version at doi:10.1016/j.jhazmat.2021.126223.

References

Bao, Y., Jiang, Y., Xiong, E., Tian, T., Zhang, Z., Lv, J., Li, Y., Zhou, X., 2020. CUT-LAMP: contamination-free loop-mediated isothermal amplification based on the CRISPR/Cas9 cleavage. ACS Sens. 5, 1082–1091.

Bulut, O., Oktem, H.A., Yilmaz, M.D., 2020. A highly substituted and fluorescent aromatic-fused imidazole derivative that shows enhanced antibacterial activity against methicillin-resistant Staphylococcus aureus (MRSA). J. Hazard. Mater. 399, 122902.

Chen, C., Li, N., Lan, J., Ji, X., He, Z., 2016. A label-free colorimetric platform for DNA via target-catalyzed hairpin assembly and the peroxidase-like catalytic of graphene/Au-NPs hybrids. Anal. Chim. Acta 902, 154–159.

Chen, H., Kou, X., Yang, Z., Ni, W., Wang, J., 2008. Shape- and size-dependent refractive index sensitivity of gold nanoparticles. Langmuir: ACS J. Surf. Colloids 24, 5233–5237.

Choi, H.M.T., Beck, V.A., Pierce, N.A., 2014. Next-generation in situ hybridization chain reaction: higher gain, lower cost, greater durability. ACS Nano 8, 4284–4294.

Cui, L., Ke, G., Zhang, W.Y., Yang, C.J., 2011. A universal platform for sensitive and selective colorimetric DNA detection based on Exo III assisted signal amplification. Biosens. Bioelectron. 26, 2796–2800.

Dirks, R.M., Pierce, N.A., 2004. From the cover: triggered amplification by hybridization chain reaction. Proc. Natl. Acad. Sci. U.S.A. 101, 15275–15278.

Gao, Z., Xu, M., Hou, L., Chen, G., Tang, D., 2013. Magnetic bead-based reverse colorimetric immunoassay strategy for sensing biomolecules. Anal. Chem. 85, 6945–6952.

Gao, Z., Hou, L., Xu, M., Tang, D., 2014. Enhanced colorimetric immunoassay accompanying with enzyme cascade amplification strategy for ultrasensitive detection of low-abundance protein. Sci. Rep. 4, 1–8.

Gao, Z., Lv, S., Xu, M., Tang, D., 2017. High-index {hk0} faceted platinum concave nanocubes with enhanced peroxidase-like activity for an ultrasensitive colorimetric immunoassay of the human prostate-specific antigen. Analyst 142, 911–917.

Gao, Z., Qiu, Z., Lu, M., Shu, J., Tang, D., 2017. Hybridization chain reaction-based colorimetric aptasensor of adenosine 5′-triphosphate on unmodified gold nanoparticles and two label-free hairpin probes. Biosens. Bioelectron. 89, 1006–1012.

Gittens-St Hilaire, M.V., Chase, E., Alleyne, D., 2020. Prevalence, molecular characteristics and antimicrobial susceptibility patterns of MRSA in hospitalized and nonhospitalized patients in Barbados. Microbes Infect. 35, 100659.

He, Z., Zhu, J., Weng, G.J., Li, J.J., Zhao, J.W., 2020. Detection of ferrous ion by etching-based multi-colorimetric sensing of gold nanobipyramids. Nanotechnology 31, 335505.

Hou, L., Wu, X., Chen, G., Yang, H., Lu, M., Tang, D., 2015. HCR-stimulated formation of DNAzyme concatamers on gold nanoparticle for ultrasensitive impedimetric immunoassay. Biosens. Bioelectron. 68, 487–493.

Hu, M., Yuan, C., Tian, T., Wang, X., Sun, J., Xiong, E., Zhou, X., 2020. Single-step, salt-aging-free, and thiol-free freezing construction of AuNP-based bioprobes for advancing CRISPR-based diagnostics. J. Am. Chem. Soc. 142, 7506–7513.

Ito, T., Okuma, K., Ma, X.X., Yuzawa, H., Hiramatsu, K., 2003. Insights on antibiotic resistance of Staphylococcus aureus from its whole genome: genomic island SCC. Drug Resist. Updates 6, 41–52.

Ji, J., Pang, Y., Li, D., Wang, X., Xu, Y., Mu, X., 2020. Single-layered graphene/Au-nanoparticles-based love wave biosensor for highly sensitive and specific detection of staphylococcus aureus gene sequences. ACS Appl. Mater. Interfaces 12, 12417–12425.

Jung, Y.K., Park, H.G., 2015. Colorimetric detection of clinical DNA samples using an intercalator-conjugated polydiacetylene sensor. Biosens. Bioelectron. 72, 127–132.

Kou, X., Zhang, S., Tsung, C.-K., Yeung, M.H., Shi, Q., Stucky, G.D., Sun, L., Wang, J., Yan, C., 2006. Growth of gold nanorods and bipyramids using CTEAB surfactant. J. Phys. Chem. B 110, 16377–16383.

Lai, W., Wei, Q., Zhuang, J., Lu, M., Tang, D., 2016. Fenton reaction-based colorimetric immunoassay for sensitive detection of brevetoxin B. Biosens. Bioelectron. 80, 249–256.

Lai, W., Wei, Q., Xu, M., Zhuang, J., Tang, D., 2017. Enzyme-controlled dissolution of MnO_2 nanoflakes with enzyme cascade amplification for colorimetric immunoassay. Biosens. Bioelectron. 89, 645–651.

Li, B., Du, Y., Li, T., Dong, S., 2009. Investigation of 3,3′,5,5′-tetramethylbenzidine as colorimetric substrate for a peroxidatic DNAzyme. Anal. Chim. Acta 651, 234–240.

Li, Q., Zhuo, X., Li, S., Ruan, Q., Xu, Q.-H., Wang, J., 2015. Production of monodisperse gold nanobipyramids with number percentages approaching 100% and evaluation of their plasmonic properties. Adv. Opt. Mater. 3, 801–812.

Li, Q., Zhou, D., Pan, J., Liu, Z., Chen, J., 2018. Ultrasensitive and simple fluorescence biosensor for detection of the mecA gene of Staphylococcus aureus by using an exonuclease III-assisted cascade signal amplification strategy. Analyst 143, 5670–5675.

Liu, M., Lee, T.W., Gray, S.K., Guyot-Sionnest, P., Pelton, M., 2009. Excitation of dark plasmons in metal nanoparticles by a localized emitter. Phys. Rev. Lett. 102, 107401.

Liu, M., Jia, C., Jin, Q., Lou, X., Yao, S., Xiang, J., Zhao, J., 2010. Novel colorimetric enzyme immunoassay for the detection of carcinoembryonic antigen. Talanta 81, 1625–1629.

Liu, M., Xiang, H., Hua, E., Wang, L., Jing, X., Cao, X., Sheng, S., Xie, G., 2014. Ultrasensitive electrochemical biosensor for the detection of the mecA gene sequence in methicillin resistant strains of staphylococcus aureusemploying gold nanoparticles. Anal. Lett. 47, 579–591.

Liu, Z., Yao, C., Wang, Y., Yang, C., 2018. A G-quadruplex DNAzyme-based LAMP biosensing platform for a novel colorimetric detection of Listeria monocytogenes. Anal. Methods 10, 848–854.

Luo, R., Li, Y., Lin, X., Dong, F., Zhang, W., Yan, L., Cheng, W., Ju, H., Ding, S., 2014. A colorimetric assay method for invA gene of Salmonella using DNAzyme probe self-assembled gold nanoparticles as single tag. Sens. Actuators B: Chem. 198, 87–93.

Nawattanapaiboon, K., Kiatpathomchai, W., Santanirand, P., Vongsakulyanon, A., Amarit, R., Somboonkaew, A., Sutapun, B., Srikhirin, T., 2015. SPR-DNA array for detection of methicillin-resistant Staphylococcus aureus (MRSA) in combination with loop-mediated isothermal amplification. Biosens. Bioelectron. 74, 335–340.

Potluri, P.R., Rajendran, V.K., Sunna, A., Wang, Y., 2020. Rapid and specific duplex detection of methicillin-resistant Staphylococcus aureus genes by surface-enhanced Raman spectroscopy. Analyst 145, 2789–2794.

Qi, Y., Zhu, J., Li, J., Zhao, J., 2016. Highly improved synthesis of gold nanobipyramids by tuning the concentration of hydrochloric acid. J. Nanopart. Res. 18, 1–16.

Saka, E., Terzi Gulel, G., 2018. Detection of enterotoxin genes and methicillin-resistance in staphylococcus aureus isolated from water buffalo milk and dairy products. J. Food Sci. 83, 1716–1722.

Sasikumar, T., Ilanchelian, M., 2020. Colorimetric and visual detection of cyanide ions based on the morphological transformation of gold nanobipyramids into gold nanoparticles. New J. Chem. 44, 4713–4718.

Shi, J., Chan, C., Pang, Y., Ye, W., Tian, F., Lyu, J., Zhang, Y., Yang, M., 2015. A fluorescence resonance energy transfer (FRET) biosensor based on graphene quantum dots (GQDs) and gold nanoparticles (AuNPs) for the detection of mecA gene sequence of Staphylococcus aureus. Biosens. Bioelectron. 67, 595–600.

Stefani, S., Chung, D.R., Lindsay, J.A., Friedrich, A.W., Kearns, A.M., Westh, H., Mackenzie, F.M., 2012. Meticillin-resistant Staphylococcus aureus (MRSA): global epidemiology and harmonisation of typing methods. Int. J. Antimicrob. Agents 39, 273–282.

Wang, H., Wu, T., Li, M., Tao, Y., 2020. Recent advances in nanomaterials for colorimetric cancer detection. J. Mater. Chem. B.

Wang, Z., Chen, Q., Zhong, Y., Yu, X., Wu, Y., Fu, F., 2019. A multicolor immunosensor for sensitive visual detection of breast cancer biomarker based on sensitive NADH-ascorbic-acid-mediated growth of gold nanobipyramids. Anal. Chem. 92, 1534–1540.

Wang, Z., Yang, L., Ye, X., Huang, C., Yang, W., Zhang, L., Wu, Z., Fu, F., 2020. Multicolor visual screening of total dithiocarbamate pesticides in foods based on sulfydryl-mediated growth of gold nanobipyramids. Anal. Chim. Acta 1139, 59–67.

Wei, J., Chen, H., Chen, H., Cui, Y., Qileng, A., Qin, W., Liu, W., Liu, Y., 2019. Multifunctional peroxidase-encapsulated nanoliposomes: bioetching-induced photoelectrometric and colorimetric immunoassay for broad-spectrum detection of ochratoxins. ACS Appl. Mater. Interfaces 11, 23832–23839.

Wu, S., Wang, Y., Duan, N., Ma, H., Wang, Z., 2015. Colorimetric aptasensor based on enzyme for the detection of vibrio parahemolyticus. J. Agric. Food Chem. 63, 7849–7854.

Xing, Y., Wang, P., Zang, Y., Ge, Y., Jin, Q., Zhao, J., Xu, X., Zhao, G., Mao, H., 2013. A colorimetric method for H1N1 DNA detection using rolling circle amplification. Analyst 138, 3457–3462.

Xu, L., Liang, W., Wen, Y., Wang, L., Yang, X., Ren, S., Jia, N., Zuo, X., Liu, G., 2018. An ultrasensitive electrochemical biosensor for the detection of mecA gene in methicillin-resistant Staphylococcus aureus. Biosens. Bioelectron. 99, 424–430.

Xu, S., Ouyang, W., Xie, P., Lin, Y., Qiu, B., Lin, Z., Chen, G., Guo, L., 2017. Highly uniform gold nanobipyramids for ultrasensitive colorimetric detection of influenza virus. Anal. Chem. 89, 1617–1623.

Xu, S., Jiang, L., Liu, Y., Liu, P., Wang, W., Luo, X., 2019. A morphology-based ultrasensitive multicolor colorimetric assay for detection of blood glucose by enzymatic etching of plasmonic gold nanobipyramids. Anal. Chim. Acta 1071, 53–58.

Xu, W., Xue, X., Li, T., Zeng, H., Liu, X., 2009. Ultrasensitive and selective colorimetric DNA detection by nicking endonuclease assisted nanoparticle amplification. Angew. Chem. Int. Ed. Engl. 48, 6849–6852.

Zhu, X., Zhuo, X., Li, Q., Yang, Z., Wang, J., 2016. Gold nanobipyramid-supported silver nanostructures with narrow plasmon linewidths and improved chemical stability. Adv. Funct. Mater. 26, 341–352.